SUPPLEMENTAL MATERIALS

Methods

Experimental animals: Transgenic (Tg) male C57BL/6 mice bearing the α-Myosin Heavy Chain (MyHC) gene containing the R403Q mutation were kindly provided by Dr. Leinwand. The R403Q-αMyHC mouse was bred on a CBA/B16 (F1) cross background (1). Transgenic (Tg) male C56BL/ 6 mice bearing a c-myc-tagged murine TnT containing the R92W mutation were kindly provided by Dr. Tardiff. The R92W-TnT mouse is an F1 cross between FVB/N and C57/B6 strains (2, 3). The R403Q-αMyHC and R92W-TnT mice were backcrossed to C57BL/6 for >10 generations. Male mice were weaned and genotyped at the age of 3 weeks by PCR-amplified tail DNA. All studies were performed at 5 weeks of age, prior to development of myocyte hypertrophy and fibrosis (1, 2, 4).

High-throughput RNA sequencing (mRNA-seq and miRNA-seq): Whole heart total RNA was prepared from three biological replicates for each genotype using miRNeasy (Qiagen). Three biological replicates each of stand-specific, poly-A+ RNA-seq libraries were constructed as described (5, 6). Paired-end 100 nt sequencing (2x 100 bp) was performed at the Beijing Genomics Institute using HiSeq2000 platform (Illumina). MiRNA-seq (small RNA-seq) libraries were prepared using size-selected 18-30 nt long RNAs by gel purification, sequenced on HiSeq2000 (Illumina), and analyzed as previously described (5, 7-10). The SRA accession number for the mRNA-seq and miRNA-seq libraries reported in this manuscript is **SRP083078.**

mRNA-seq data analysis: Approximately 19-24 million paired-end fragment reads were obtained for each library; the statistics are summarized in Supplemental Table S1. Approximately 94-97% of the paired reads were mapped to the mm10 mouse genome using TopHat on the Galaxy platform (11, 12). The differential expression of a total 23963 annotated nuclear-encoded genes was analyzed using Cufflinks and Cuffdiff on the Galaxy platform (11, 12). Mitochondrial genes, whose mRNA levels are exceptionally high, were not included in the differential expression analysis as in most mRNA-seq studies, since even small changes in their levels can prevent accurate estimation of the abundance and changes of the mRNA levels of nuclear-encoded genes. The results of differential expression analysis are summarized in Supplemental Table S2. Please see Supplemental Data section for detailed methods.

miRNA-seq analysis: Approximately 13-18 million reads were obtained for each library; the statistics are summarized in Supplemental Table S5. Approximately 60-80% of the reads were mapped to the mm9 mouse genome, of which ~19-27% were mapped to miRNA hairpins. The abundance of each mature miRNA normalized by the sequencing depth (total genome-mapping reads) in each library was calculated. Then the mean abundance of each miRNA among the biological replicates was calculated. The normalized miRNA abundance in each library and the mean abundance among the biological replicates are summarized in Supplemental Table S6. To eliminate miRNAs with very low expression levels, which are unlikely to have a physiological role, only miRNAs (n=92) whose mean abundance was more

than 100 reads per million total reads in at least one of the four mice were analyzed in Figure 3.

qRT-PCR of miRNAs: qRT-PCR of miRNAs was performed using TaqMan Advanced miRNA assay kit (ThermoFischer) following the manufacturer's instructions.

Adult myocyte isolation: Cardiac myocytes were isolated from 5 week old mouse hearts, using a published protocol (13, 14). Briefly, mice were heparinized (100 IU heparin) 10 min prior to cervical dislocation. The hearts were rapidly excised, cannulated via the aorta, and perfused in the langendorf mode with a constant perfusion pressure of 80 mm Hg. The hearts were then perfused for 10 min using Ca^{2+}-free Tyrode containing (in mM) NaCl (120), KCl (5.4), NaH_2PO_4 (1.2), $NaHCO_3$ (20), $MgCl_2$ (1.6), glucose (1 mg/ml), 2, 3-butanedione monoxime (BDM, 1 mg/ml), taurine (0.628 mg/ml), 0.9 mg/ml collagenase type 2 (Worthington Biochemical Co., 299 U/mg), and gassed with 95% O_2–5% CO_2. The heart was then cut into small pieces and gently agitated, allowing myocytes to be dispersed in the Ca^{2+}-free Tyrode containing BSA (5 mg/l) for 10 min. Dispersed myocytes were filtered through a 150 µm mesh and gently centrifuged at 500 rpm for 30 sec. The cells were re-suspended in Ca^{2+}-containing buffers, with Ca^{2+} concentrations gradually increasing from 0.125 to 1 mM Ca^{2+}, and stored in 1 mM Ca^{2+} solution until use.

Two photon microscopy to assess cellular redox status in isolated cardiac myocytes: Experiments were performed at 37°C in a thermostatically controlled flow chamber mounted on the stage of an upright microscope (Nikon E600FN) attached to a multi-photon laser scanning system with excitation at 740 nm (13-15). Cells were suspended in Tyrode solution, pH 7.4, containing (in mM), NaCl (140), KCl (5), MgCl2 (1), HEPES (10), CaCl2 (1), and glucose (10). TMRM (tetramethylrhodamine methyl esther, 100 nM, red λ_{em} 605 ± 25 nm) and MCB (monochlorobimane, 50 uM, blue λ_{em} 480 ± 20nm) were loaded for 20 min on the stage of the microscope at 37°C to simultaneously monitor mitochondrial ($\Delta\Psi_m$) and reduced glutathione (GSH) respectively. Autofluorescence of NAD(P)H, namely total fluorescence collected at <490 nm, was monitored separately. The acquired signal was calibrated by the addition of KCN for maximum reduction of existing NAD(P)H, followed by addition of FCCP for maximum oxidation of NADPH. Image analysis was performed using Image J software.

Quantification of mitochondrial DNA copy number: Total nucleic acids were extracted from hearts using the Tissue Lyzer disruption system. The homogenate was treated with 1.6 mg/ml RNase A (Qiagen) for 10 minutes at room temperature and then with proteinase K for 20 min at 55 ºC. In order to purify total heart DNA, the digests were mixed with ethanol and loaded on DNeasy columns, using the manufacturer's (Qiagen) protocol. The DNA concentration was quantified using a spectrophotometer (Nanodrop). Twenty nanograms of DNA were used as template in Taqman-based quantitative real-time PCR. The gene-specific assay for mtDNA was Mm04225243_g1 for

murine cytochrome-c oxidase subunit 1 (COX-I) and Mm99999915_g1 for glyceraldehyde phosphate dehydrogenase (GAPDH, nuclear gene), from Life Technologies were used as previously described (16). The amount of COX-I relative to GAPDH was calculated according to the ΔCt method and normalized (ΔΔCt) to littermate control heart values to obtain a measure of mtDNA in the different samples.

Mitochondrial Isolation: Isolation and handling of mitochondria was performed as previously described (15, 17, 18). Mice were euthanized by cervical dislocation, hearts were harvested and immersed in ice cold isolation solution (IS, pH 7.4, containing (in mM) Sucrose (75), Mannitol (225), EGTA (1)). Ventricles were homogenized in IS with the addition of 0.1 mg/ml bacterial proteinase (type XXIV, Sigma-Aldrich), followed by 0.2% albumin (fatty acid-free) to block proteinase activity. Homogenate was then centrifuged at 500 g for 10 min to discard unbroken tissue and debris. The supernatant was centrifuged at 10,000 g for 10 min to sediment the mitochondria and then washed twice using IS by centrifuging at 7,700 g for 5 min. The mitochondrial pellet was re-suspended in Suspension Solution (IS without EGTA) and protein concentration was determined using the bicinchoninic acid method (BCA protein assay kit, Thermo Fisher Scientific).

Measurement of mitochondrial respiration: Respiration was evaluated in freshly isolated mitochondria using an automated 96-well extracellular flux analyzer (Seahorse XF96; Seahorse Bioscience, Billerica, MA) and Buffer B

(pH 7.2) containing (in mM) KCl (137), KH_2PO_4 (2), EGTA (0.5), $MgCl_2$ (2.5), HEPES (20) with 0.2% fatty acid-free BSA (14, 18). Mitochondria were assayed in polyethyleneimine-coated XF96 plates. After removing the polyethyleneimine (1:15,000 dilution in buffer B, overnight incubation at 37°C without CO_2), 10 µg of mitochondrial protein was transferred to each well and centrifuged at 3,000 g for 7 min at 4^{o}C, before starting the assay. Mitochondrial respiration from substrates of Complex I was evaluated by robotic injection of 5 mM each of glutamate and malate (GM) to determine State 4 respiration; 1 mM ADP was added to assess State 3 respiration. Succinate (5mM) with Rotenone (1µM) followed with/without ADP was used to evaluate Complex II respiration and TMPD (N,N,N′,N′-Tetramethyl-p-phenylenediamine, 0.5 mM) for Complex IV respiration.

Measurement of mitochondrial membrane potential (ΔΨm), **ROS generation and ROS scavenging capacity:** NAD(P)H redox status, mitochondrial swelling and $\Delta\psi_m$ were monitored simultaneously using a wavelength-scanning fluorometer (QuantaMaster; Photon Technology International, Inc.) and multidye program (15, 18). Isolated mitochondria were suspended in buffer B (same as above, without BSA). For each assay, 150 µg of mitochondrial protein was suspended in 2 ml of buffer B in a quartz cuvette with a stirring bar at 37 ^{o}C. NAD(P)H autofluorescence ($\lambda_{exc:}$340, λ_{em}:450 nm) and mitochondrial swelling (90° light scattering λ_{exc}=520, λ_{em}:585 nm) were monitored. NAD(P)H signal was calibrated with the addition of KCN (2.5 mM) for maximal reduction and 2,4-dinitrophenol (DNP, 20 µM) for minimal reduction. The % of NAD(P)H reduced was then estimated during State 4 and

State 3 (Supplemental Figure S3A). Δψm was recorded using tetramethylrhodamine methyl ester (TMRM; 100 nM) by applying the ratiometric method of Scaduto and Grotyohann (19) which uses λ_{exc}: 546 nm and 573 nm, and λ_{em}: 590 nm.

Amplex Red (AR) from Life Technologies was used to measure H_2O_2 production by isolated mitochondria (14, 15) (Supplemental Figure 3B, C). Mitochondrial suspensions (150 µg) with added 10 µM AR and Horseradish peroxidase (1 U/ml, HRP, Sigma) were loaded in 2 ml Buffer B in a quartz cuvette with a stirring bar at 37 ^{o}C. Resorufin, the fluorescent product obtained by the 1:1 stoichiometric oxidative reaction of horseradish conjugated-AR with H_2O_2 was monitored at λ_{exc}=530 nm and λ_{em}= 590 nm. Glutamate/malate (5 mM) was used to measure ROS generation via Forward Electron Transport (NADH dependent respiration, through Complex I) (Supplemental Figure S3B) and succinate (5 mM) + rotenone (1 µM, Complex I inhibitor) was used to assess Complex I Reverse Electron Transport (Supplemental Figure S3C). Glutamate/malate (5/5 mM) or succinate (5 mM) were used to measure ROS generation during state 4 respiration; ADP (1 mM) was added to measure ROS generation during state 3 respiration. At the end of the experiment, calibration of the AR signal was achieved with 100 picomoles H_2O_2. Quantification of the H_2O_2 produced was based on estimation of the slope of the AR signal. [H_2O_2] (during state 4 or state 3 respiration)= slope of AR (during state 4 or 3) *100(pmoles)/calibration slope/mitochondrial protein used x 60seconds/duration of measurement (state 4 or 3), as previously described (15).

In order to evaluate ROS scavenging capacity by the glutathione and thioredoxin systems in isolated mitochondria (18), Auranofin (50 nM, Sigma) and dinitrochlorobenzene (DNCB, 10 μM, Sigma) were used to inhibit selectively the thioredoxin and glutathione pathways respectively in the inter-membrane space and mitochondrial matrix, while H_2O_2 emission was recorded. Initially both inhibitors were used in order to achieve maximum ROS emission, with no scavenging. Then, selective blockade with each inhibitor permitted us to estimate the extent of scavenging by each system (Supplemental Figure S3D).

Measurement of mitochondrial Calcium handling: Mitochondria (~600μg) were suspended in a buffer (pH 7.2) containing (in mM) KCl (137), KH_2PO_4 (2), EGTA (0.02) and HEPES (20, 21). Extra-mitochondrial and intra-mitochondrial [Ca^{++}] were measured simultaneously using Calcium Green-5N (0.1 μM, hexopotassium salt, cell impermeant, Life Technologies; λ_{exc}:505, λ_{em}:535nm) and Fura-FF(λ_{exc}:340 and 380nm, λ_{em}:510nm), respectively. In order to quantify mitochondrial matrix $[Ca^{++}]_{free}$, isolated mitochondria were loaded with Fura-FF (20 μM incubation for 30 min at room temperature followed by washing 2-3 times with SS as described above). The Fura-FF signal was calibrated by treating mitochondria with the Ca^{++} ionophore 4-bromo-A23187 (2 μM), oligomycin (5 μg/ml) and FCCP (5 μM) to allow equilibration between intra- and extra-mitochondrial Ca^{++}. The calibration curve was established according to the equation: $[Ca^{2+}]=K_d'\beta\ (R- R_{min})/(R_{max} - R)$ where R is the ratio of λ_{em}:510nm intensities for λ_{exc}: 340 and 380 nm. K_d' is the apparent Ca-fura-FF dissociation constant, and β is the fluorescence

intensity ratio for Ca^{++}-free and Ca^{++}-saturated fura-FF excited at 380 nm. R_{max} and R_{min} are R values for Ca^{++}-saturated and Ca^{++}-free Fura-FF. The experiment was performed in energized mitochondria (at State 4, with GM) at room temperature. Repeated additions of [Ca^{+2}] (5 μM) were performed at 1 min intervals (Supplemental Figure S3E). Total [Ca^{+2}] until PTP opened and matrix $[Ca^{++}]_{free}$ were calculated using the online version of WEBMAXC (http://maxchelator.stanford.edu/webmaxc/webmaxcE.htm). Mitochondrial permeability transition pore opening was characterized by abrupt collapse of $\Delta\psi_m$, swelling and changes in recorded [Ca^{++}], namely, a decrease in the Fura-FF signal and increase in the Ca Green signal.

References

1. Vikstrom KL, Factor SM, Leinwand LA. Mice expressing mutant myosin heavy chains are a model for familial hypertrophic cardiomyopathy. Molecular medicine (Cambridge, Mass). 1996;2(5):556-67. Epub 1996/09/01. PubMed PMID: 8898372; PubMed Central PMCID: PMCPMC2230192.
2. Ertz-Berger BR, He H, Dowell C, Factor SM, Haim TE, Nunez S, et al. Changes in the chemical and dynamic properties of cardiac troponin T cause discrete cardiomyopathies in transgenic mice. Proceedings of the National Academy of Sciences of the United States of America. 2005;102(50):18219-24. Epub 2005/12/06. doi: 10.1073/pnas.0509181102. PubMed PMID: 16326803; PubMed Central PMCID: PMCPMC1298915.
3. Tardiff JC, Hewett TE, Palmer BM, Olsson C, Factor SM, Moore RL, et al. Cardiac troponin T mutations result in allele-specific phenotypes in a mouse model for hypertrophic cardiomyopathy. The Journal of clinical investigation. 1999;104(4):469-81. Epub 1999/08/17. doi: 10.1172/jci6067. PubMed PMID: 10449439; PubMed Central PMCID: PMCPMC408522.
4. Geisterfer-Lowrance AA, Christe M, Conner DA, Ingwall JS, Schoen FJ, Seidman CE, et al. A mouse model of familial hypertrophic cardiomyopathy. Science (New York, NY). 1996;272(5262):731-4. Epub 1996/05/03. PubMed PMID: 8614836.
5. Fukunaga R, Han BW, Hung JH, Xu J, Weng Z, Zamore PD. Dicer partner proteins tune the length of mature miRNAs in flies and mammals. Cell. 2012;151(3):533-46. doi: 10.1016/j.cell.2012.09.027. PubMed PMID: 23063653; PubMed Central PMCID: PMC3609031.
6. Zhang Z, Theurkauf WE, Weng Z, Zamore PD. Strand-specific libraries for high throughput RNA sequencing (RNA-Seq) prepared without poly(A) selection. Silence. 2012;3(1):9. doi: 10.1186/1758-907X-3-9. PubMed PMID: 23273270; PubMed Central PMCID: PMC3552703.

7. Fukunaga R, Colpan C, Han BW, Zamore PD. Inorganic phosphate blocks binding of pre-miRNA to Dicer-2 via its PAZ domain. The EMBO journal. 2014;33(4):371-84. doi: 10.1002/embj.201387176. PubMed PMID: 24488111.
8. Han BW, Wang W, Li C, Weng Z, Zamore PD. Noncoding RNA. piRNA-guided transposon cleavage initiates Zucchini-dependent, phased piRNA production. Science. 2015;348(6236):817-21. doi: 10.1126/science.aaa1264. PubMed PMID: 25977554; PubMed Central PMCID: PMC4545291.
9. Han BW, Wang W, Zamore PD, Weng Z. piPipes: a set of pipelines for piRNA and transposon analysis via small RNA-seq, RNA-seq, degradome- and CAGE-seq, ChIP-seq and genomic DNA sequencing. Bioinformatics (Oxford, England). 2015;31(4):593-5. Epub 2014/10/25. doi: 10.1093/bioinformatics/btu647. PubMed PMID: 25342065; PubMed Central PMCID: PMCPMC4325541.
10. Kandasamy SK, Fukunaga R. Phosphate-binding pocket in Dicer-2 PAZ domain for high-fidelity siRNA production. Proceedings of the National Academy of Sciences of the United States of America. 2016;113(49):14031-6. Epub 2016/11/23. doi: 10.1073/pnas.1612393113. PubMed PMID: 27872309; PubMed Central PMCID: PMCPMC5150366.
11. Trapnell C, Roberts A, Goff L, Pertea G, Kim D, Kelley DR, et al. Differential gene and transcript expression analysis of RNA-seq experiments with TopHat and Cufflinks. Nature protocols. 2012;7(3):562-78. doi: 10.1038/nprot.2012.016. PubMed PMID: 22383036; PubMed Central PMCID: PMC3334321.
12. Afgan E, Baker D, van den Beek M, Blankenberg D, Bouvier D, Cech M, et al. The Galaxy platform for accessible, reproducible and collaborative biomedical analyses: 2016 update. Nucleic acids research. 2016;44(W1):W3-w10. Epub 2016/05/04. doi: 10.1093/nar/gkw343. PubMed PMID: 27137889; PubMed Central PMCID: PMCPMC4987906.
13. Tocchetti CG, Wang W, Froehlich JP, Huke S, Aon MA, Wilson GM, et al. Nitroxyl improves cellular heart function by directly enhancing cardiac sarcoplasmic reticulum Ca2+ cycling. Circulation research. 2007;100(1):96-104. Epub 2006/12/02. doi: 10.1161/01.RES.0000253904.53601.c9. PubMed PMID: 17138943; PubMed Central PMCID: PMCPMC2769513.
14. Tocchetti CG, Caceres V, Stanley BA, Xie C, Shi S, Watson WH, et al. GSH or palmitate preserves mitochondrial energetic/redox balance, preventing mechanical dysfunction in metabolically challenged myocytes/hearts from type 2 diabetic mice. Diabetes. 2012;61(12):3094-105. Epub 2012/07/19. doi: 10.2337/db12-0072. PubMed PMID: 22807033; PubMed Central PMCID: PMCPMC3501888.
15. Aon MA, Cortassa S, O'Rourke B. Redox-optimized ROS balance: a unifying hypothesis. Biochimica et biophysica acta. 2010;1797(6-7):865-77. Epub 2010/02/24. doi: 10.1016/j.bbabio.2010.02.016. PubMed PMID: 20175987; PubMed Central PMCID: PMCPMC2891851.
16. Papanicolaou KN, Kikuchi R, Ngoh GA, Coughlan KA, Dominguez I, Stanley WC, et al. Mitofusins 1 and 2 are essential for postnatal metabolic remodeling in heart. Circulation research. 2012;111(8):1012-26. Epub 2012/08/21. doi: 10.1161/circresaha.112.274142. PubMed PMID: 22904094; PubMed Central PMCID: PMCPMC3518037.
17. Aon MA, Cortassa S, Maack C, O'Rourke B. Sequential opening of mitochondrial ion channels as a function of glutathione redox thiol status. The Journal of biological chemistry. 2007;282(30):21889-900. Epub 2007/06/02. doi: 10.1074/jbc.M702841200. PubMed PMID: 17540766; PubMed Central PMCID: PMC2292488.
18. Aon MA, Stanley BA, Sivakumaran V, Kembro JM, O'Rourke B, Paolocci N, et al. Glutathione/thioredoxin systems modulate mitochondrial H2O2 emission: an experimental-computational study. The Journal of general physiology. 2012;139(6):479-91. Epub

2012/05/16. doi: 10.1085/jgp.201210772. PubMed PMID: 22585969; PubMed Central PMCID: PMCPMC3362521.
19. Scaduto RC, Jr., Grotyohann LW. Measurement of mitochondrial membrane potential using fluorescent rhodamine derivatives. Biophysical journal. 1999;76(1 Pt 1):469-77. Epub 1999/01/06. doi: 10.1016/s0006-3495(99)77214-0. PubMed PMID: 9876159; PubMed Central PMCID: PMCPMC1302536.
20. Wei AC, Liu T, Cortassa S, Winslow RL, O'Rourke B. Mitochondrial Ca2+ influx and efflux rates in guinea pig cardiac mitochondria: low and high affinity effects of cyclosporine A. Biochimica et biophysica acta. 2011;1813(7):1373-81. Epub 2011/03/03. doi: 10.1016/j.bbamcr.2011.02.012. PubMed PMID: 21362444; PubMed Central PMCID: PMCPMC3109245.
21. Wei AC, Liu T, Winslow RL, O'Rourke B. Dynamics of matrix-free Ca2+ in cardiac mitochondria: two components of Ca2+ uptake and role of phosphate buffering. The Journal of general physiology. 2012;139(6):465-78. Epub 2012/05/30. doi: 10.1085/jgp.201210784. PubMed PMID: 22641641; PubMed Central PMCID: PMCPMC3362519.

RESULTS

Supplemental Figure S1: Cardiac pathology of mutant and littermate control mice.

Representative microscopy images with Masson's trichrome staining (10X and 40X magnification) from R403Q-αMyHC (MHC), R92W-TnT (TNT) and littermate control 5 week male mice (CON-MHC and CON-TNT). No evidence of fibrosis, myocyte disarray or hypertrophy are observed**.**

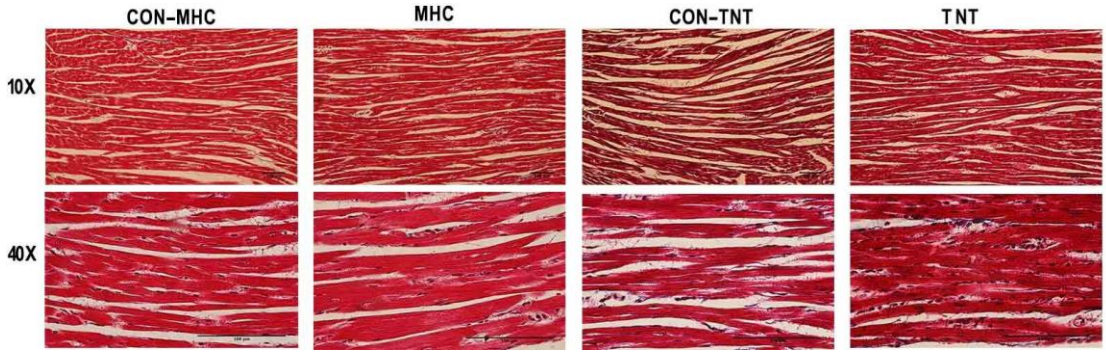

Supplemental Figure S2: Differentially expressed mRNAs of genes encoding proteins involved in ROS generation/scavenging and cellular and mitochondrial calcium level regulation.

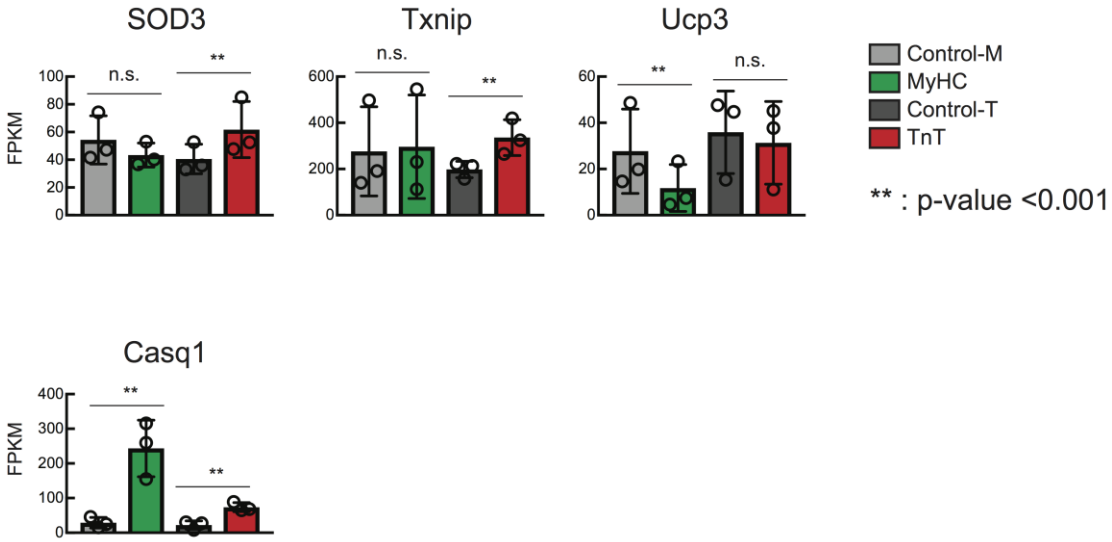

Differentially expressed mRNA levels (Fragments Per Kilobase of exon per Million fragments mapped, FPKM) of genes involved in (A) ROS generation or scavenging and in (B) cellular and mitochondrial calcium level regulation revealed by mRNA-seq. Mean +/- S.D. (n=3 biological replicates); * and ** represent p-value <0.01 and <0.001, respectively, using two-sided student's t-test.

Supplemental Figure S3 : Representative fluorometry traces in isolated mitochondria

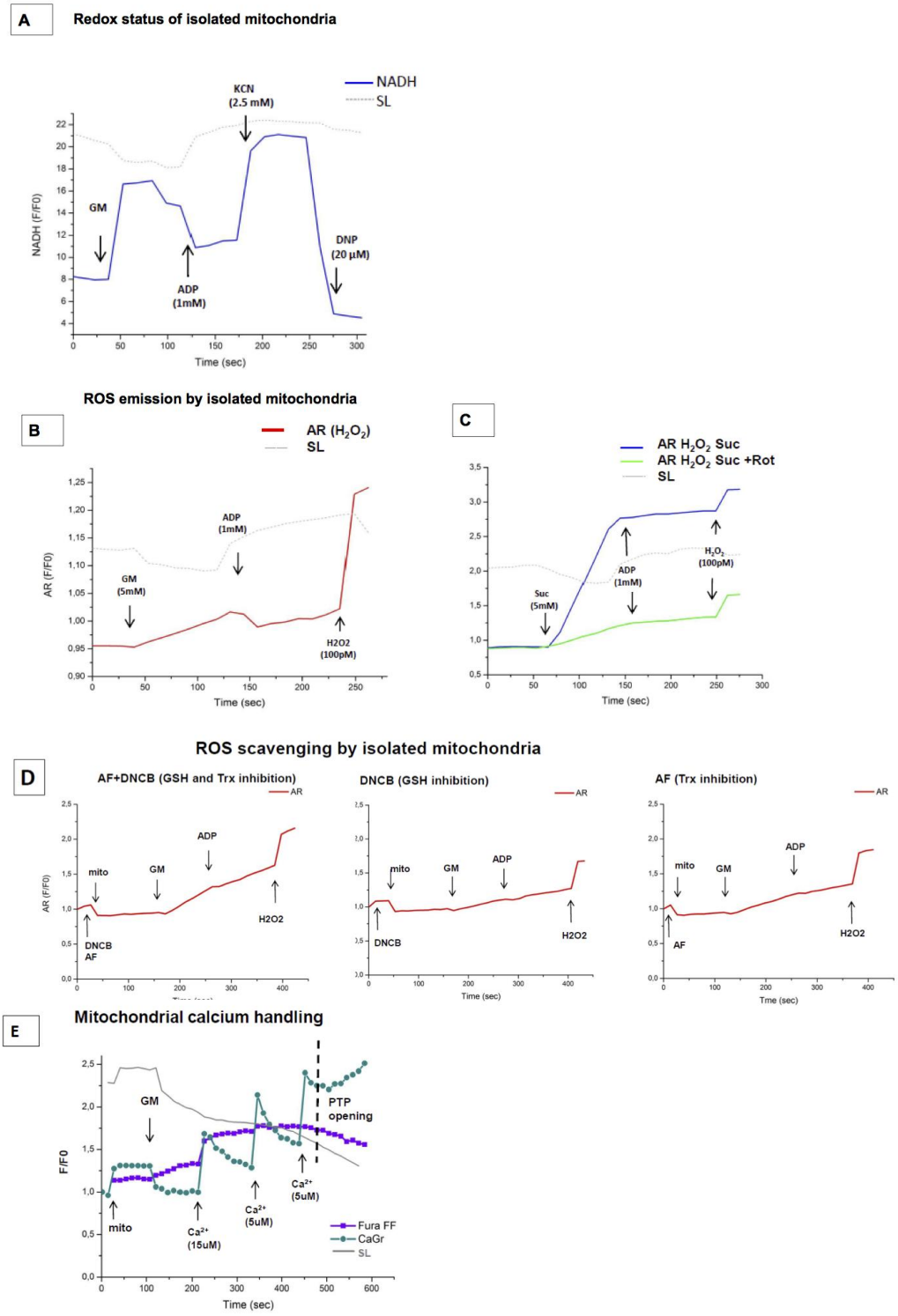

(A) Estimation of NAD(P)H in control mitochondria. The blue line ($\lambda_{exc:}$340, λ_{em}:450 nm, blue line) tracks changes in NAD(P)H (λ_{exc}:340, λ_{em}:450 nm) and the grey line reflects changes in mitochondrial volume (90^{o} scattered light, SL). NAD(P)H and SL were monitored following the addition of 5mM glutamate/malate (State 4), followed by 100mM ADP (State 3). Estimation of the NAD(P)H pool was achieved by addition of potassium cyanide (KCN, 2.5mM) for maximal reduction of NAD(P)H and 2,4-dinitrophenol (DNP, 20μM) for minimal reduction.

(B, C) H_2O_2 emission was monitored using 10μM Amplex Red (λ_{exc}:530 nm and λ_{em}: 590 nm) following addition of glutamate/malate (GM/5mM), succinate (Suc/5mM) and succinate following rotenone (Suc/5mM and Rot/1μM); a merged figure is provided for Suc and Suc+Rot. ADP addition (100mM) initiated State 3 respiration. At the end of the experiment, H_2O_2 (100 pM) was added to assist with quantification of ROS emission. Changes in mitochondrial volume were monitored (grey scattered line, 90^{o} scattered light, SL).

(D) ROS scavenging: H_2O_2 generation by control mitochondria monitored using 10μM Amplex Red (λ_{exc}=530 nm, λ_{em}= 590 nm), in the presence of glutamate/malate (GM) following inhibition of the glutathione (GSH) and thioredoxin (Trx) systems by Auranofin (AF, 50 nM) and dinitrolchlorobenzene (DNCB, 10μM) respectively.

(E) Mitochondrial calcium handling: Mitochondria were pre-incubated with Fura-FF (20μM) to monitor intra-mitochondrial [Ca^{2+}] changes. Calcium Green-5N (0.1 μM) was added at the beginning of the experiment to monitor extra-mitochondrial [Ca^{2+}] changes. Mitochondria were energized with glutamate/malate (5mM). Additions of $CaCl_2$ followed. End of the experiment

was marked by activation of Permeability Transition Pore (PTP) opening, reflected by abrupt increase of the Calcium Green signal (λ_{exc}:505, λ_{em}:535nm, green line), decrease of Fura-FF signal (ratio of λ_{exc} 340/380nm, λ_{em}:510nm, purple line) and marked mitochondrial swelling (grey line, 90^{o} scattered light, SL)

Supplemental Table 1. Sequencing statistics of mRNA-seq.

Genotype	Total reads	% Mapping			SRA accession number
		1st read	2nd read	Pairs	
Control-M, R1	22172955	98,2	98,5	97,0	SRR4070097
Control-M, R2	20765590	98,0	98,3	96,7	SRR4070098
Control-M, R3	24254204	98,0	98,4	96,7	SRR4070099
MyHC-R403Q mutant, R1	20436048	97,0	97,5	95,9	SRR4070092
MyHC-R403Q mutant, R2	21883740	95,5	96,0	93,9	SRR4070094
MyHC-R403Q mutant, R3	21302286	96,1	96,7	94,6	SRR4070095
Control-T, R1	18856511	97,7	98,1	96,2	SRR4070089
Control-T, R2	23323656	97,9	98,3	96,5	SRR4070090
Control-T, R3	21578970	98,0	98,2	96,5	SRR4070091
TnT-R92W mutant, R1	21966888	97,2	97,6	95,5	SRR4070086
TnT-R92W mutant, R2	20870631	97,5	97,8	95,9	SRR4070087
TnT-R92W mutant, R3	23321178	97,1	97,4	95,3	SRR4070088

R1, R2, and R3 are biological replicates

Supplemental Table 2. Differential expression analysis of mRNA-seq. Cuffdiff outputs are shown. (see in a separate file)

Supplemental Table 3. KEGG pathway and GO term enrichment analysis using WebGestalt of differentially expressed genes identified by mRNA-seq.

	Changed in MyHC		Changed in TnT	
	KEGG/GO Term	**Adjusted p-value**	**KEGG/GO term**	**Adjusted p-value**
KEGG pathway	Calcium signaling pathway	2,0E-04	ECM-receptor interaction	3,9E-11
	Toxoplasmosis	2,0E-04	Focal adhesion	8,5E-08
	Insulin signaling pathway	2,0E-04	Protein digestion and absorption	8,9E-06
	PPAR signaling pathway	4,0E-04	Hypertrophic cardiomyopathy (HCM)	1,0E-04
	Amoebiasis	4,0E-04	Amoebiasis	1,0E-04
	Hypertrophic cardiomyopathy (HCM)	3,4E-03	Malaria	5,0E-04
	Metabolic pathways	3,4E-03	TGF-beta signaling pathway	6,0E-04
	ECM-receptor interaction	3,4E-03	Rheumatoid arthritis	6,0E-04
	Dilated cardiomyopathy	3,7E-03	Pathways in cancer	6,0E-04
	Fatty acid biosynthesis	4,1E-03	Dilated cardiomyopathy	6,0E-04
	Arginine and proline metabolism	4,1E-03	Chagas disease (American trypanosomiasis)	1,2E-03
	Focal adhesion	4,1E-03	Adipocytokine signaling pathway	1,6E-03
	Biosynthesis of unsaturated fatty acids	4,1E-03	Osteoclast differentiation	2,6E-03
	Tyrosine metabolism	1,2E-02	Tryptophan metabolism	2,6E-03
	Malaria	2,1E-02	MAPK signaling pathway	2,6E-03
	Melanogenesis	2,7E-02	Insulin signaling pathway	5,3E-03
	Pathways in cancer	3,9E-02	GnRH signaling pathway	6,9E-03
	Nitrogen metabolism	4,3E-02	Colorectal cancer	7,9E-03
	Leishmaniasis	4,3E-02	Toxoplasmosis	1,7E-02
	Long-term potentiation	4,5E-02	Bladder cancer	2,0E-02
	MAPK signaling pathway	4,5E-02	Small cell lung cancer	2,1E-02
	Adipocytokine signaling pathway	4,5E-02	Type II diabetes mellitus	2,6E-02
	Axon guidance	4,6E-02	Leishmaniasis	5,2E-02
	Hepatitis C	5,2E-02	Vascular smooth muscle contraction	6,0E-02
	Regulation of actin cytoskeleton	5,6E-02	Metabolic pathways	6,9E-02
	Rheumatoid arthritis	5,6E-02	Complement and coagulation cascades	6,9E-02
	Small cell lung cancer	6,0E-02	Citrate cycle (TCA cycle)	6,9E-02
	Alanine, aspartate and glutamate metabolism	6,0E-02	Chronic myeloid leukemia	6,9E-02
	Glycine, serine and threonine metabolism	6,0E-02	PPAR signaling pathway	7,1E-02
	Gap junction	6,1E-02	Cardiac muscle contraction	7,1E-02
	Fructose and mannose	6,5E-02	Apoptosis	7,8E-02

	metabolism			
	Pyrimidine metabolism	6,9E-02	Prion diseases	7,8E-02
	Purine metabolism	6,9E-02	Regulation of actin cytoskeleton	8,0E-02
	GnRH signaling pathway	7,0E-02		
	Toll-like receptor signaling pathway	7,0E-02		
	Chagas disease (American trypanosomiasis)	7,0E-02		
	Pyruvate metabolism	7,0E-02		
	Tryptophan metabolism	7,6E-02		
GO term (biological process)	small molecule metabolic process	4,1E-07	extracellular matrix organization	6,7E-16
	cellular process	4,1E-07	extracellular structure organization	6,7E-16
	response to chemical stimulus	4,1E-07	developmental process	1,5E-14
	regulation of multicellular organismal process	4,1E-07	system development	9,8E-14
	negative regulation of biological process	4,1E-07	multicellular organismal development	1,7E-13
	cellular response to cytokine stimulus	6,4E-07	anatomical structure development	1,3E-12
	response to stress	6,4E-07	cell adhesion	2,5E-12
	innate immune response	2,4E-06	biological adhesion	2,9E-12
	response to stimulus	2,4E-06	tissue development	3,2E-11
	regulation of localization	2,4E-06	organ development	1,3E-10
	biological regulation	3,2E-06	response to chemical stimulus	1,4E-10
	phosphorus metabolic process	3,8E-06	response to endogenous stimulus	3,1E-10
	heart process	4,7E-06	anatomical structure formation involved in morphogenesis	4,2E-10
	organonitrogen compound metabolic process	4,7E-06	anatomical structure morphogenesis	8,4E-10
	heart contraction	4,7E-06	circulatory system development	2,7E-09
	developmental process	4,7E-06	cardiovascular system development	2,7E-09
	regulation of heart contraction	6,7E-06	cell differentiation	2,7E-09
	muscle contraction	7,0E-06	blood vessel development	4,8E-09
	regulation of cell communication	7,0E-06	skeletal system development	4,9E-09
	response to cytokine stimulus	7,0E-06	cellular component organization	6,9E-09
	response to organic substance	7,0E-06	vasculature development	7,9E-09
	metabolic process	7,0E-06	response to organic substance	1,2E-08
	multicellular organismal development	1,3E-05	cell-substrate adhesion	1,9E-08
	system development	1,3E-05	cellular response to chemical stimulus	2,9E-08
	regulation of signaling	1,4E-05	cellular component organization or biogenesis	2,9E-08
	regulation of molecular function	1,4E-05	cellular developmental process	3,0E-08
	phosphate-containing compound metabolic process	1,4E-05	cell migration	3,4E-08

	circulatory system process	1,4E-05	cell development	4,3E-08
	blood circulation	1,4E-05	response to organic nitrogen	6,8E-08
	defense response to virus	1,6E-05	collagen fibril organization	8,0E-08
	cellular metabolic process	1,7E-05	single-multicellular organism process	8,8E-08
	single-multicellular organism process	1,7E-05	multicellular organismal process	9,6E-08
	multicellular organismal process	1,7E-05	single-organism process	1,1E-07
	single-organism process	1,7E-05	localization of cell	1,6E-07
	regulation of system process	1,9E-05	cell motility	1,6E-07
	muscle system process	1,9E-05	positive regulation of developmental process	2,8E-07
	negative regulation of cellular process	1,9E-05	cellular component movement	3,9E-07
	striated muscle contraction	2,4E-05	cellular response to organic nitrogen	4,0E-07
	cell proliferation	2,9E-05	locomotion	6,2E-07
	regulation of biological quality	3,7E-05	cellular process	6,7E-07
GO term (molecular function)	protein binding	5,7E-11	binding	3,6E-14
	binding	6,9E-09	carbohydrate derivative binding	1,8E-13
	anion binding	1,6E-07	glycosaminoglycan binding	2,3E-13
	ion binding	3,1E-06	heparin binding	4,3E-13
	small molecule binding	5,8E-05	protein binding	3,0E-12
	nucleoside phosphate binding	2,0E-04	ion binding	5,7E-09
	nucleotide binding	2,0E-04	extracellular matrix structural constituent	1,3E-08
	purine ribonucleotide binding	2,0E-04	fibronectin binding	2,9E-08
	ribonucleotide binding	2,0E-04	calcium ion binding	1,3E-06
	purine nucleotide binding	2,0E-04	extracellular matrix binding	3,2E-06
	adenyl nucleotide binding	6,0E-04	collagen binding	5,1E-06
	adenyl ribonucleotide binding	6,0E-04	extracellular matrix constituent conferring elasticity	2,5E-05
	receptor binding	7,0E-04	endopeptidase activity	2,9E-05
	ribonucleoside binding	8,0E-04	receptor binding	3,2E-05
	purine ribonucleoside triphosphate binding	8,0E-04	growth factor binding	3,3E-05
	nucleoside binding	8,0E-04	metallopeptidase activity	3,3E-05
	purine ribonucleoside binding	8,0E-04	anion binding	4,7E-05
	purine nucleoside binding	8,0E-04	identical protein binding	6,5E-05
	oxidative phosphorylation uncoupler activity	9,0E-04	peptidase activity	7,9E-05
	voltage-gated cation channel activity	1,0E-03	metal ion binding	8,2E-05
	heparin binding	1,0E-03	integrin binding	9,0E-05
	carbohydrate derivative binding	1,0E-03	metalloendopeptidase activity	1,0E-04
	carboxylic acid binding	2,9E-03	peptidase activity, acting on L-amino acid peptides	1,0E-04
	ATP binding	2,9E-03	cation binding	2,0E-04
	glycosaminoglycan binding	3,6E-03	growth factor activity	2,0E-04

	transferase activity, transferring phosphorus-containing groups	4,1E-03	protein homodimerization activity	1,0E-03
	catalytic activity	4,1E-03	insulin-like growth factor binding	1,0E-03
	cAMP binding	4,1E-03	cytoskeletal protein binding	1,9E-03
	voltage-gated ion channel activity	5,3E-03	actin binding	1,9E-03
	voltage-gated channel activity	5,3E-03	peptidase activator activity	2,6E-03
	stearoyl-CoA 9-desaturase activity	5,9E-03	protein-lysine 6-oxidase activity	2,6E-03
	double-stranded RNA binding	6,2E-03	protein complex binding	2,6E-03
	RNA polymerase II regulatory region sequence-specific DNA binding	6,2E-03	oxidoreductase activity, acting on the CH-NH2 group of donors, oxygen as acceptor	4,1E-03
	cytoskeletal protein binding	6,7E-03	catalytic activity	4,8E-03
	acyl-CoA desaturase activity	7,2E-03	calcium-dependent protein binding	5,7E-03
	insulin-like growth factor binding	7,6E-03	protein dimerization activity	5,7E-03
	RNA polymerase II regulatory region DNA binding	8,0E-03	oxidoreductase activity	5,7E-03
	kinase activity	9,9E-03	oxidoreductase activity, acting on the CH-NH2 group of donors	5,7E-03
	RNA polymerase II core promoter sequence-specific DNA binding	9,9E-03	structural molecule activity	6,3E-03
	growth factor activity	1,0E-02	peptidase regulator activity	7,5E-03
GO term (cellular component)	myofibril	2,4E-08	extracellular matrix	2,3E-37
	contractile fiber	3,6E-08	extracellular region part	3,3E-35
	extracellular region part	9,2E-08	extracellular region	7,0E-35
	cytoplasm	9,4E-08	proteinaceous extracellular matrix	9,0E-32
	sarcomere	9,4E-08	extracellular matrix part	3,1E-22
	contractile fiber part	2,1E-07	extracellular space	3,9E-22
	proteinaceous extracellular matrix	3,3E-07	collagen	3,6E-14
	extracellular matrix	1,6E-06	basement membrane	1,0E-08
	extracellular matrix part	3,3E-06	contractile fiber	7,1E-07
	extracellular space	4,0E-06	contractile fiber part	9,3E-07
	cell part	4,4E-06	myofibril	1,9E-06
	cell	4,4E-06	sarcomere	2,6E-06
	extracellular region	6,5E-06	cytoplasm	2,6E-06
	intracellular part	1,2E-05	I band	1,2E-05
	cytoplasmic part	2,2E-05	cytoplasmic part	2,4E-05
	intracellular	2,3E-05	fibrillar collagen	7,1E-05
	basement membrane	2,4E-05	cell part	7,0E-04
	I band	2,5E-05	cell	7,0E-04
	laminin-5 complex	2,6E-05	intracellular	8,0E-04
	neuronal cell body	2,0E-04	intracellular part	8,0E-04
	laminin complex	5,0E-04	sarcolemma	8,0E-04
	cell body	5,0E-04	collagen type I	8,0E-04

	myosin complex	1,4E-03	actin cytoskeleton	1,6E-03
	actin cytoskeleton	1,4E-03	endoplasmic reticulum	2,9E-03
	perinuclear region of cytoplasm	2,0E-03	cell periphery	2,9E-03
	T-tubule	2,3E-03	cation channel complex	5,5E-03
	dendrite	2,3E-03	plasma membrane	7,3E-03
	cytosol	2,3E-03	perinuclear region of cytoplasm	7,7E-03
	neuron projection	2,3E-03	fibrinogen complex	9,8E-03
	lipid particle	3,3E-03	sheet-forming collagen	9,8E-03
	cytoskeleton	3,7E-03	collagen type IV	9,8E-03
	basal lamina	4,0E-03	plasma membrane part	1,1E-02
	cytoskeletal part	4,0E-03	Z disc	1,1E-02
	Z disc	4,3E-03	cell body	1,9E-02
	axon	4,3E-03	membrane	1,9E-02
	cell junction	5,5E-03	myosin complex	2,0E-02
	mitochondrial inner membrane	5,8E-03	mitochondrial inner membrane	2,1E-02
	protein complex	6,6E-03	organelle envelope	2,5E-02
	axon terminus	7,2E-03	caveola	2,7E-02
	organelle inner membrane	7,7E-03	envelope	2,7E-02

Supplemental Table 4. Differentially expressed mRNAs of genes involved in metabolism**.**

Gene name	Assciated GO terms related with metabolism	Change in MyHC	Change in TnT
Acaca	acetyl-CoA metabolic process fatty acid metabolic process lipid metabolic process metabolic process multicellular organismal protein metabolic process	Downregulated in MyHC	
Acad11	metabolic process		Downregulated in TnT
Ace	beta-amyloid metabolic process peptide metabolic process regulation of angiotensin metabolic process		Upregulated in TnT
Acot1	acyl-CoA metabolic process long-chain fatty acid metabolic process	Downregulated in MyHC	
Adipoq	fatty acid oxidation glucose metabolic process negative regulation of gluconeogenesis positive regulation of cellular protein metabolic process positive regulation of fatty acid metabolic process regulation of glucose metabolic process	Downregulated in MyHC	Downregulated in TnT
Aebp1	peptide metabolic process		Upregulated in TnT
Agtpbp1	neurotransmitter metabolic process	Downregulated in MyHC	
Alas2	metabolic process porphyrin-containing compound metabolic process	Downregulated in MyHC	
Aldh1a2	metabolic process retinal metabolic process retinoic acid metabolic process retinoid metabolic process		Upregulated in TnT
Aldh6a1	metabolic process thymine metabolic process valine metabolic process		Downregulated in TnT
Ankrd23	fatty acid metabolic process	Upregulated in MyHC	Upregulated in TnT
Apod	glucose metabolic process lipid metabolic process	Upregulated in MyHC	
Asns	glutamine metabolic process	Upregulated in MyHC	
Atf3	gluconeogenesis	Upregulated in MyHC	
Bckdhb	metabolic process		Downregulated in TnT

Bdh1	metabolic process	Downregulated in MyHC	
Car3	one-carbon metabolic process	Downregulated in MyHC	Downregulated in TnT
Car5b	one-carbon metabolic process		Downregulated in TnT
Cdo1	taurine metabolic process	Downregulated in MyHC	
Ces1d	acyl-CoA metabolic process lipid metabolic process medium-chain fatty acid metabolic process	Downregulated in MyHC	Downregulated in TnT
Ctgf	reactive oxygen species metabolic process	Upregulated in MyHC	Upregulated in TnT
Cyp1b1	arachidonic acid metabolic process benzene-containing compound metabolic process cellular aromatic compound metabolic process dibenzo-p-dioxin metabolic process estrogen metabolic process positive regulation of reactive oxygen species metabolic process regulation of reactive oxygen species metabolic process retinal metabolic process retinol metabolic process steroid metabolic process toxin metabolic process xenobiotic metabolic process		Upregulated in TnT
Cyp2e1	drug metabolic process heterocycle metabolic process monoterpenoid metabolic process steroid metabolic process triglyceride metabolic process xenobiotic metabolic process	Downregulated in MyHC	Downregulated in TnT
Cyr61	reactive oxygen species metabolic process	Upregulated in MyHC	Upregulated in TnT
Dct	metabolic process	Upregulated in MyHC	#N/A
Dgat2	diacylglycerol metabolic process glycerol metabolic process lipid metabolic process long-chain fatty-acyl-CoA metabolic process negative regulation of fatty acid oxidation positive regulation of gluconeogenesis regulation of lipoprotein metabolic process		Downregulated in TnT
Dio2	thyroid hormone metabolic process		Upregulated in TnT
Enpp2	lipid metabolic process metabolic process	Downregulated in MyHC	
Enpp6	choline metabolic process		Upregulated in TnT

	lipid metabolic process metabolic process		
Fah	aromatic amino acid family metabolic process metabolic process	Downregulated in MyHC	Downregulated in TnT
Fam213b	fatty acid metabolic process lipid metabolic process prostaglandin metabolic process	Upregulated in MyHC	
Fasn	acetyl-CoA metabolic process fatty acid metabolic process fatty acid synthase activity lipid metabolic process metabolic process	Downregulated in MyHC	Downregulated in TnT
Fbp2	carbohydrate metabolic process fructose 1,6-bisphosphate metabolic process fructose 6-phosphate metabolic process fructose metabolic process gluconeogenesis metabolic process	Downregulated in MyHC	
Foxo3	regulation of reactive oxygen species metabolic process	Downregulated in MyHC	
Gcdh	acyl-CoA metabolic process fatty acid oxidation metabolic process		Downregulated in TnT
Glul	glutamate metabolic process nitrogen compound metabolic process	Upregulated in MyHC	
Gpd1	carbohydrate metabolic process gluconeogenesis glycerol-3-phosphate metabolic process glycerolipid metabolic process NADH metabolic process	Downregulated in MyHC	
Hmgcs2	cholesterol metabolic process lipid metabolic process metabolic process steroid metabolic process	Downregulated in MyHC	
Hmox1	heme metabolic process		Upregulated in TnT
Hsd17b7	lipid metabolic process		Downregulated in TnT
Igfbp5	glucose metabolic process regulation of glucose metabolic process	Downregulated in MyHC	
Il15	hyaluronan metabolic process		Downregulated in TnT
Inmt	amine metabolic process	Downregulated in MyHC	
Lrat	1,2-diacyl-sn-glycero-3-phosphocholine metabolic process retinol metabolic process	Downregulated in MyHC	Downregulated in TnT

	vitamin A metabolic process		
Maob	positive regulation of dopamine metabolic process	Downregulated in MyHC	
Mfap4	regulation of collagen metabolic process		Upregulated in TnT
Mgst1	glutathione metabolic process	Downregulated in MyHC	Downregulated in TnT
Mmp3	negative regulation of hydrogen peroxide metabolic process		Upregulated in TnT
Mthfd2	metabolic process one-carbon metabolic process tetrahydrofolate metabolic process	Upregulated in MyHC	
Myc	glucose metabolic process positive regulation of oxidative phosphorylation regulation of oxidative phosphorylation		Upregulated in TnT
Myh7	ATP metabolic process	Upregulated in MyHC	Upregulated in TnT
Nme1	nucleotide metabolic process purine nucleotide metabolic process pyrimidine nucleotide metabolic process	Upregulated in MyHC	
Odc1	polyamine metabolic process	Upregulated in MyHC	
Ogdhl	tricarboxylic acid cycle		Downregulated in TnT
P3h2	collagen metabolic process		Upregulated in TnT
Pck1	gluconeogenesis glucose metabolic process lipid metabolic process oxaloacetate metabolic process	Downregulated in MyHC	Downregulated in TnT
Pfkfb1	fructose 2,6-bisphosphate metabolic process fructose metabolic process metabolic process	Downregulated in MyHC	Downregulated in TnT
Phkg1	carbohydrate metabolic process glycogen metabolic process	Downregulated in MyHC	
Plin1	lipid metabolic process	Downregulated in MyHC	
Pm20d1	cellular amino acid metabolic process cellular lipid metabolic process metabolic process regulation of oxidative phosphorylation uncoupler activity		Downregulated in TnT
Pnpla3	lipid metabolic process metabolic process	Downregulated in MyHC	
Prkag3	fatty acid metabolic process lipid metabolic process	Upregulated in MyHC	Upregulated in TnT
Prkar2b	fatty acid metabolic process	Downregulated in MyHC	Downregulated in TnT
Rbp1	retinoic acid metabolic process retinol metabolic process		Upregulated in TnT

	vitamin A metabolic process		
Scd1	fatty acid metabolic process lipid metabolic process triglyceride metabolic process	Downregulated in MyHC	Downregulated in TnT
Scd4	fatty acid metabolic process lipid metabolic process	Downregulated in MyHC	
Sod3	superoxide metabolic process		Upregulated in TnT
Star	cellular lipid metabolic process glucocorticoid metabolic process		Upregulated in TnT
Tecrl	lipid metabolic process		Downregulated in TnT
Thbs1	negative regulation of plasma membrane long-chain fatty acid transport positive regulation of reactive oxygen species metabolic process regulation of cGMP metabolic process		Upregulated in TnT
Tlr4	leukotriene metabolic process	Upregulated in MyHC	
Uck2	metabolic process pyrimidine nucleobase metabolic process	Upregulated in MyHC	Upregulated in TnT
Ucp1	oxidative phosphorylation uncoupler activity	Downregulated in MyHC	
Ucp3	fatty acid metabolic process oxidative phosphorylation uncoupler activity	Downregulated in MyHC	
Ung	metabolic process		Downregulated in TnT

Supplemental Table 5. Pathway analysis using IPA using mRNA-seq data.

(see in a separate file)

Supplemental Table 6. Sequencing statistics of miRNA-seq.

Genotype	Total reads	rRNA mapping reads	MicroRNA hairpin-mapping reads	Genome mapping reads (– rRNA; +miRNA hairpin)	Genome mapping reads (– rRNA; – miRNA hairpin)	Genome unique mapping reads (– rRNA; +miRNA hairpin)	Genome unique mapping reads (– rRNA; – miRNA hairpin)	SRA accession number
Control-M, R1	16783086	12868	2904261	13571861	10667600	3304266	400005	SRR4070105
Control-M, R2	17895842	21721	3123108	14307304	11184196	3744232	621124	SRR4070106
Control-M, R3	14922003	12922	3072094	11845475	8773381	3527403	455309	SRR4070085
MyHC-R403Q mutant, R1	13298971	11576	1650736	8078515	6427779	2012890	362154	SRR4070102
MyHC-R403Q mutant, R2	14101076	18046	1694432	8628377	6933945	2155411	460979	SRR4070103
MyHC-R403Q mutant, R3	13739162	14584	1707516	8420902	6713386	2104752	397236	SRR4070104
Control-T, R1	14307835	31103	2077070	10844448	8767378	3020923	943853	SRR4070096
Control-T, R2	15991706	19489	3372955	12557911	9184956	3785547	412592	SRR4070100
Control-T, R3	18397103	19446	3096084	14422410	11326326	3604128	508044	SRR4070101
TnT-R92W mutant, R1	16458555	54539	2370391	11694142	9323751	3376629	1006238	SRR4070083
TnT-R92W mutant, R2	15292348	61681	2534448	10255580	7721132	3283522	749074	SRR4070084

R1, R2, and R3 are biological replicates

Supplemental Table 7. Expression of miRNAs revealed by miRNA-seq (see in a separate file). Normalized reads (reads per million non-rRNA-mapping reads) are shown.